Cell cycle control and bifurcation for a free boundary problem modeling tissue growth

Wenrui Hao* Bei Hu† Andrew J. Sommese‡

April 30, 2012

Abstract

We consider a free boundary problem for a system of partial differential equations, which arise in a model of cell cycle with a free boundary. For the quasi steady state system, it depends on a positive parameter β, which describes the signals from the microenvironment. Upon discretizing this model, we obtain a family of polynomial systems parameterized by β. We numerically find that there exists a radially-symmetric stationary solution with boundary $r = R$ for any given positive number R by using numerical algebraic geometry method. By homotopy tracking with respect to the parameter β, there exist branches of symmetry-breaking stationary solutions. Moreover, we proposed a numerical algorithm based on Crandall-Rabinowitz theorem to numerically verify the bifurcation points. By continuously changing β using a homotopy, we are able to compute nonradial symmetric solutions. We additionally discuss control function β.

keyword Bifurcation, free boundary problem, polynomial systems, homotopy continuation, cell cycle.

1 Introduction

Multicell spheroids used in tumor growth models have been developed and studied for a number of years. Basic multicellular spheroid models are based on a central necrotic core, an inner shell of quiescent cells and an outer rim of proliferating, viable cells. Early models were produced by Burton [7] and Greenspan [22, 23], which described the growth of multicellular spheroids by modeling nutrient supply and cell volume growth and loss. Since then a variety of tumor

*Department of Applied and Computational Mathematics and Statistics, University of Notre Dame, Notre Dame, IN 46556 (whao@nd.edu, www.nd.edu/∼whao). This author was supported by the Dunces Chair of the University of Notre Dame.

†Department of Applied and Computational Mathematics and Statistics, University of Notre Dame, Notre Dame, IN 46556 (b1hu@nd.edu, www.nd.edu/∼b1hu).

‡Department of Applied and Computational Mathematics and Statistics, University of Notre Dame, Notre Dame, IN 46556 (sommese@nd.edu, www.nd.edu/∼sommese). This author was supported by the Dunces Chair of the University of Notre Dame.

models appeared in the literature, taking into account various avascular and vascularized stages of tumor development, etc, see [8, 9, 10, 11, 29] and the references therein. More recently, [32] presented a model including mitosis of labeled cells, and [30] modeled the quiescent and proliferating sub-populations as different cell cycle states with conversion from one state to another decadent upon local nutrient concentration.

For free boundary problems in tumor models, there are a series of papers [6, 13, 18, 19, 20, 14, 15, 16, 17, 21] that deal with bifurcation analysis and multiscale models for tumors with free boundary. For the tumor model where Darcy's law is used, local existence and uniqueness were proved in [6]. In [21] it was proved that for a reasonable range of parameters, there exists a unique radially-symmetric stationary solution. In [13] it was proved in the 3-dimensional case that there exists a sequence of symmetric-breaking of stationary solutions bifurcating from the tumor aggressiveness parameter μ_n $(n = 2, 3, 4, \ldots)$.

For a multiscale tumor model, it is proved in [18] that there exists a unique global-in-time solution to the system of PDEs and free boundary $r = R(t)$ of the multiscale model. In [17], it showed that an important gene APC effects the free boundary. In [15], the existence of the non-trivial steady state solution has been proved.

In the past several years, simulation of tumor models has increased dramatically. Nonlinear modeling has been performed to study the effects of shape instabilities on avascular [12], vascular and angiogenic [27, 33] solid tumor growth. A new, adaptive boundary integral method to simulate the three dimensional solid tumor growth was developed in [28]. A computational method to deal with a high-dimension, multiscale models was developed in [1]. Moreover, [24, 26, 25] provide an efficient method to directly solve steady state systems for free boundary problem.

In this paper, we are studying tumor model of the cell cycle clock with a free boundary developed in [18]. This model is spatially multiscale in the sense that it includes gene mutations at the cell level and cells densities in the tumor region; thus the model combines genetic information with continuous mechanics. The model considers two time-scales: the usual time of tumor growth and the cycling time of cells, although the cycling time varies in discrete steps. We computed the radial symmetric solution of steady state system using algorithms from numerical algebraic geometry and proposed a general numerical algorithmic approach to verify the bifurcation point. Control on β and tracking on non-radial symmetric branches are also implemented.

2 Mathematical model

There exist four phases in the eucaryotic cell cycle, mitosis (M), synthesis (S), gap 1 (G_1) and gap 2 (G_2). The DNA is replicated in the S-phase. During the M-phase the nucleus membrane breaks down, sister chromatids are separated, new nucleus membranes are formed, and the daughter cells split. The G_1-phase is the interval between the completion of the M-phase and the beginning of

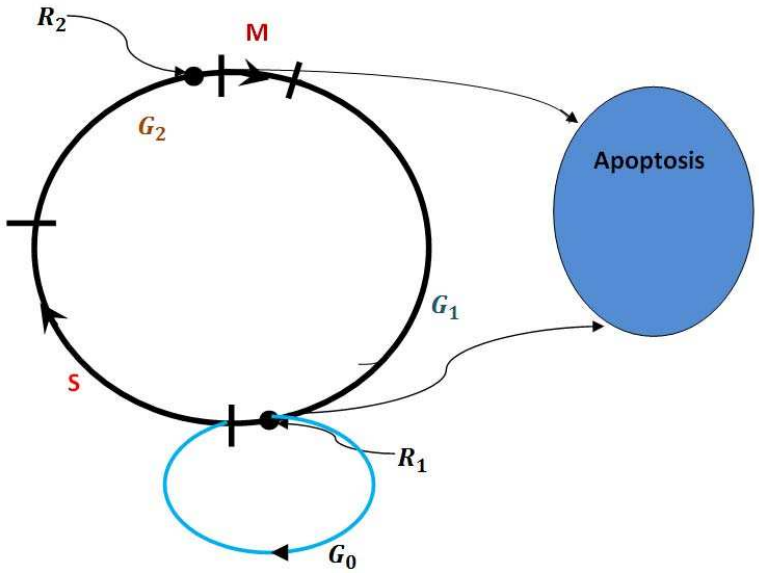

Figure 1: Phases of the eukaryotic cell cycle

the S-phase, and the G_2 is the interval between the end of the S-phase and the beginning of the M-phase. Moreover, there are two check points in the cell cycle: the R_1 checkpoint and the R_2 checkpoint. These points are also called "restriction" points. At the checkpoint R_1, a cell decides whether to continue to the S phase, transit to quiescence mode G_0, or, in case of irreparable damage, undergo apoptosis. There are two important genes that control the pathway to cell proliferation: SMAD and APC. At the restriction point R_1, SMAD shuts off the pathway to proliferation under hypoxic conditions, while APC does the same thing if the microenvironment is overpopulated, then they send the cell into quiescence model G_0. See [17] for more detail about SMAD and APC. At the second checkpoint R_2, a cell checks if the DNA has been correctly duplicated, in case of damage, the cell may undergo apoptosis. Figure 1 shows the diagram of the eukaryotic cell cycle and the decision a cell makes at the check points R_1 and R_2.

Let $p_1(\mathbf{x}, t, s_1)$ be density of cells in phase G_1, $s_1 \in [0, A_1]$; $p_2(\mathbf{x}, t, s_2)$ be density of cells in phase S and G_2, $s_2 \in [0, A_2]$; $p_3(\mathbf{x}, t, s_3)$ be density of cells in phase M, $s_3 \in [0, A_3]$; $p_0(\mathbf{x}, t, s_0)$ be density of cells in state G_0, $s_0 \in [0, A_0]$; and $p_4(\mathbf{x}, t)$ be density of necrotic (dead) cells. Here $\mathbf{x}$ varies in the domain Ω_t. We denote by $w(\mathbf{x}, t)$ the oxygen concentration. Due to cell proliferation and death, there is a velocity field $\vec{v}(\mathbf{x}, t)$, which for simplicity is assumed to be

common to all the cells. By conservation of mass,

$$\frac{\partial p_i}{\partial t} + \frac{\partial p_i}{\partial s_i} + \mathrm{div}(p_i \vec{v}) = \lambda_i(w) p_i, \text{ for } 0 < s_i < A_i (i = 1, 2, 3), \tag{1}$$

$$\frac{\partial p_0}{\partial t} + \frac{\partial p_0}{\partial s_i} + \mathrm{div}(p_0 \vec{v}) = -\lambda_0 p_0, \text{ for } 0 < s_0 < A_0, \tag{2}$$

$$\frac{\partial p_i}{\partial t} + \mathrm{div}(p_4 \vec{v}) = \mu_1 p_1(\mathbf{x}, t, A_1) + \mu_2 p_2(\mathbf{x}, t, A_2) - \lambda_4 p_4 \tag{3}$$

where $\lambda_i(w)$ are growth rates which depend on the oxygen concentration w, $\lambda_i(w) > 0$ for $i = 1, 2, 3$. The growth rate is proportional to the amount of oxygen w when w is small and is bounded for large w. Therefore, we choose the Michaelis-Menten function:

$$\lambda_i(w) = \lambda(w) = \frac{\lambda^* w}{1 + w},$$

where λ^* is a constant. λ_0 is the death rate of cells in quiescence mode, λ_4 is the clearing rate of dead cells, and μ_1, μ_2 are the rates at which cells at R_1 and R_2, respectively, decide to go into apoptosis, and $\mu_1 < 1, \mu_2 < 1$. We also have the following period conditions:

$$p_1(\mathbf{x}, t, 0) = p_3(\mathbf{x}, t, A_3), \tag{4}$$

$$p_2(\mathbf{x}, t, 0) = [1 - \beta(t) - \mu_1] p_1(\mathbf{x}, t, A_1) + p_0(\mathbf{x}, t, A_0), \tag{5}$$

$$p_3(\mathbf{x}, t, 0) = (1 - \mu_2) p_2(\mathbf{x}, t, A_2), \tag{6}$$

$$p_0(\mathbf{x}, t, 0) = \beta(t) p_1(\mathbf{x}, t, A_1), \tag{7}$$

where $\beta(\mathbf{x}, t)$ function is viewed as a function controlling the rate going into quiescence state, $0 < \beta(\mathbf{x}, t) < 1 - \mu_1$. At the check point R_1, there is a fraction $\beta(t)$ of the cells goes into quiescence while a fraction μ_1 goes into apoptosis, and the remaining cells with the cells from the quiescence period go to the S phase, so that (5) holds.

We introduce the total density of each population of life cells:

$$Q_i(\mathbf{x}, t) = \int_0^{A_i} p_i(\mathbf{x}, t, s_i) ds_i, (i = 0, 1, 2, 3), \mathbf{x} \in \Omega_t$$

and formally set $Q_4(\mathbf{x}, t) = p_4(\mathbf{x}, t)$. Then the density of live cells which are not in quiescent phase

$$Q(\mathbf{x}, t) = \sum_{i=1}^{3} Q_i(\mathbf{x}, t),$$

and the total density of all cells is assumed to be constant, i.e.,

$$\sum_{i=0}^{4} Q_i(\mathbf{x}, t) = \text{const.} = C,$$

here we take $C = 1$ after normalization. We integrate each of the equations in (1) and (2) over $s_i \in (0, A_i)$, and sum up the resulting equations and (3). Combing the period conditions (4)-(7), we obtain

$$\sum_{i=0}^{4} \left[\frac{\partial Q_i}{\partial t} + \mathrm{div}(Q_i \vec{v}) \right] = \sum_{i=1}^{3} \lambda_i(w) Q_i - \lambda_0 Q_0 - \lambda_4 Q_4,$$

or

$$\mathrm{div}(\vec{v}) = \sum_{i=1}^{3} \lambda_i(w) Q_i - \lambda_0 Q_0 - \lambda_4 Q_4. \tag{8}$$

The pressure π is related to the velocity $\vec{v}$ of the concentration, and assuming Darcy's law in the tissue, we have

$$\vec{v} = -\nabla \pi. \tag{9}$$

Then the cell-to-cell adhesiveness condition at the tumor boundary is represented by

$$\pi = \gamma \kappa \text{ on } \partial\Omega_t,$$

where κ is the mean curvature of the surface $\partial\Omega_t$. Furthermore, the continuity condition $\vec{v} \cdot \vec{n} = V_n$ yields the relation

$$V_n = -\frac{\partial \pi}{\partial n} \qquad \text{on } \partial\Omega_t \tag{10}$$

where n is the outward normal and V_n is the velocity of the free boundary $\partial\Omega_t$ in the direction n.

Finally we assume that the oxygen concentration $w(\mathbf{x}, t)$ satisfies the diffusion equation

$$-\Delta w(\mathbf{x}, t) + (Q(\mathbf{x}, t) + Q_0(\mathbf{x}, t)) w(\mathbf{x}, t) = 0, \text{ in } \Omega_t.$$

We prescribe a boundary condition

$$w(\mathbf{x}, t) = \bar{w} \text{ on } \partial\Omega_t.$$

For simplicity, let's introduce a function

$$p(\mathbf{x}, t, s) = \begin{cases} (1 - \mu_2) p_2(\mathbf{x}, t, s), & 0 \le s \le A_2, \\ p_3(\mathbf{x}, t, s - A_2), & A_2 \le s \le A_2 + A_3, \\ p_3(\mathbf{x}, t, s - A_2 - A_3), & A_2 + A_3 \le s \le A_1 + A_2 + A_3 \equiv A, \end{cases}$$

so that

$$Q(\mathbf{x}, t) = \frac{1}{1 - \mu_2} \int_0^{A_2} p(\mathbf{x}, t, s) ds + \int_{A_2}^{A} p(\mathbf{x}, t, s) ds.$$

Parameter	Value
λ^*	$10ln2$ day^{-1}
λ_0	$\frac{ln2}{10}$ day^{-1}
λ_4	$\frac{1}{2}$ day^{-1}
μ_1	$\frac{1}{5}$

Parameter	Value
A	1 day
$A_i (i = 1, 2, 3)$	$\frac{1}{3}$day
A_0	5 days
μ_2	$\frac{1}{5}$

Table 1: Parameter values

3 Quasi-stationary solution

The model has two time scale. Each level addresses a phenomenon over a specific window of time. The quasi-steady-state system of the model of cell cycle is given by setting t-derivatives to be 0. Then the quasi steady state system becomes

$$\begin{cases} \frac{\partial p(\mathbf{x},s)}{\partial s} - \nabla p(\mathbf{x},s)\cdot\nabla\pi(\mathbf{x}) - p(\mathbf{x},s)\Delta\pi(\mathbf{x}) = \lambda(w)p(\mathbf{x},s), 0 < s < A \\ \frac{\partial p_0(\mathbf{x},s)}{\partial s} - \nabla p_0(\mathbf{x},s)\cdot\nabla\pi(\mathbf{x}) - p_0(\mathbf{x},s)\Delta\pi(\mathbf{x}) = -\lambda_0 p_0(\mathbf{x},s), 0 < s < A_0 \\ -\nabla p_4(\mathbf{x})\cdot\nabla\pi(\mathbf{x}) - p_4(\mathbf{x})\Delta\pi(\mathbf{x}) = \mu_1 p(\mathbf{x},A) + \frac{\mu_2}{1-\mu_2}p(\mathbf{x},A_2) - \lambda_4 p_4(\mathbf{x}) \\ \Delta\pi(\mathbf{x}) = \lambda(w)Q(\mathbf{x}) - \lambda_0 Q_0(\mathbf{x}) - \lambda_4 p_4(\mathbf{x}) \\ -\Delta w(\mathbf{x}) + (Q(\mathbf{x}) + Q_0(\mathbf{x}))w(\mathbf{x}) = 0 \\ w(\mathbf{x}) = \bar{w}, \text{ on } \partial\Omega \\ \frac{\partial\pi(\mathbf{x})}{\partial n} = 0, \text{ on } \partial\Omega \\ \pi(\mathbf{x}) = \gamma\kappa, \text{ on } \partial\Omega \end{cases} \tag{11}$$

with the period condition

$$\begin{cases} p(\mathbf{x},0) = (1-\mu_2)[1-\mu_1-\beta]p(\mathbf{x},A) + (1-\mu_2)p_0(\mathbf{x},A_0) \\ p_0(\mathbf{x},0) = \beta p(\mathbf{x},A) \end{cases}. \tag{12}$$

In the below section we explore numerically radial and non-radial symmetric solutions, how the choice of the control $\beta(\mathbf{x})$ can be improved to achieve the quasi-stationary solutions by time marching. We take the parameter values from [17] listed in Table 1:

4 Radial symmetric solution

4.1 $p = e^{as}p(r,\theta)$ and $p_0 \equiv 0$

The system is complex, we first consider a simplified case $p = e^{as}p(r,\theta)$ and $p_0 \equiv 0$. Then (12) becomes

$$\begin{cases} p(r,\theta) = (1-\mu_2)[1-\mu_1-\beta]p(r,\theta)e^{aA} \\ 0 = \beta p(r,\theta)e^{aA} \end{cases},$$

which implies that

$$\beta = 0 \text{ and } (1-\mu_2)(1-\mu_1)e^{aA} = 1.$$

Then $a = -\dfrac{\ln\big((1-\mu_1)(1-\mu_2)\big)}{A}$ and the radial symmetric case of the system (11) becomes

$$\begin{cases} ap - p_r\pi_r - \left(\pi_{rr} + \dfrac{2}{r}\pi_r\right)p = \lambda(w)p, 0 < s < A \\ -p_{4r}\pi_r - \left(\pi_{rr} + \dfrac{2}{r}\pi_r\right)p_4 = \mu_1 p(A) + \dfrac{\mu_2}{1-\mu_2}p(A_2) - \lambda_4 p_4 \\ -\pi_{rr} - \dfrac{2}{r}\pi_r = \lambda(w)(\dfrac{1}{a(1-\mu_2)}(e^{aA_2}-1) + \dfrac{1}{a}(e^{aA} - e^{aA_2}))p - \lambda_4 p_4 \\ -w_{rr} - \dfrac{2}{r}w_r + \left(\dfrac{1}{a(1-\mu_2)}(e^{aA_2}-1) + \dfrac{1}{a}(e^{aA} - e^{aA_2})\right)pw = 0 \\ \pi(R) = \dfrac{\gamma}{R} \\ w(R) = \bar{w} \\ \pi_r(R) = 0 \end{cases} . \quad (13)$$

This system is discretized using the third order finite difference scheme for both interior equations and boundary conditions [24, 26]. Quasi steady state solution to the simplified boundary value problem (13) were found by computing all solutions of the resulting polynomial system of equations using the software package Bertini [2, 3] for the number of grid points $N = 6$. Bertini is a software package in the field of numerical algebraic geometry that implements homotopy continuation based algorithms to numerically compute all solutions of polynomial systems over $\mathbb{C}$. For more information on homotopy continuation and the field of numerical algebraic geometry, see [31]. This discretized polynomial system has an obvious *multihomogeneous* structure [31], here we list the Beźout number for different homogeneous treatments in Table 2, where N is the number of grid points. Therefore, the optimal decomposition is $\{p_i, p_{4_i}\} \times \{\pi_i\} \times \{w_i\}$. For $N = 6$, we used Bertini with adaptive precision tracking [4, 5] to solve the discretized polynomial system. We ran Bertini on a cluster consisting of a manager that uses one core of a Xeon 5410 processor and up to 20 computing nodes, each containing two Xeon 5410 processors running 64-bit Linux, i.e., each node consists of 8 processing cores. Then we refined the solutions with finer grids using the Newton method. Table 3 lists the number of real solutions, the number of computing nodes utilized, and the time needed to compute all solutions of the discretized polynomial system. The only one real solution is plotted in Figure 2.

4.2 Homotopy tracking with respect to β

Upon computing the radially symmetric solution for $\beta = 0$ with the assumption $p = e^{as}p(r)$ and $p_0 \equiv 0$, the second step is to utilize the parameterizations by β of the discretized system of (11) to find the nontrivial solution, namely, $p_0 \neq 0$.

Multihomogeneous treatment	Bezout number		
$(i = 1, \cdots, N)$	$N = 4$	$N = 5$	$N = 6$
$\{p_i\} \times \{p_{4i}\} \times \{\pi_i\} \times \{w_i\}$	231,504	7,880,900	260,121,672
$\{p_i, p_{4i}, \pi_i\} \times \{w_i\}$	121,920	4,000,900	133,170,408
$\{p_i, p_{4i}\} \times \{\pi_i, w_i\}$	48,450	468,325	4,222,764
$\{p_i, p_{4i}\} \times \{\pi_i\} \times \{w_i\}$	27,236	325,565	3,811,230

Table 2: Summary of Bezout number of the discretized system for different N

N	# of real sol.	nodes	time
6	148	20	23h54m
12	24	10	5m54s
24	10	3	2m23s
48	2	1	3m12s
96	1	serial	5m21s
192	1	serial	7m52s

Table 3: Summary of solving the discretized system for different N

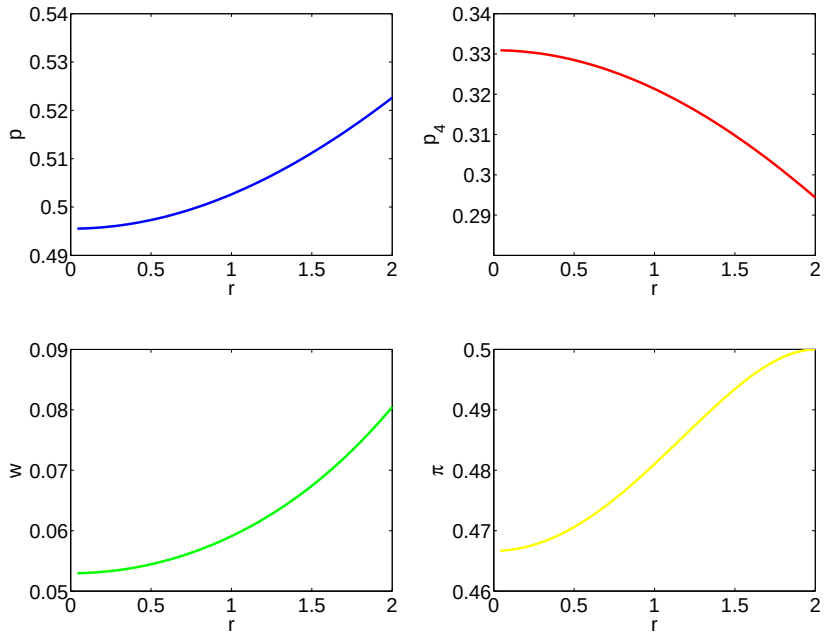

Figure 2: radial symmetric solution for (13) with $N = 192$

We utilized parameter continuation implemented in Bertini to look for other solutions as β varied from 0 to $1-\mu_1$. Figure 3 displays a graph of a nontrivial radial solutions for (11) with respect to $\beta = 0.1$. The density distribution is shown in 4. And the cell density of mitosis phase increases exponentially since cell growth stops at this stage and cellular energy is focused on the orderly division into two daughter cells. While cells increase in size (G_1 phase), replicate DNA (S phase) and continue to grow (G_2 phase) so that the cell density is not increasing during the interphase.

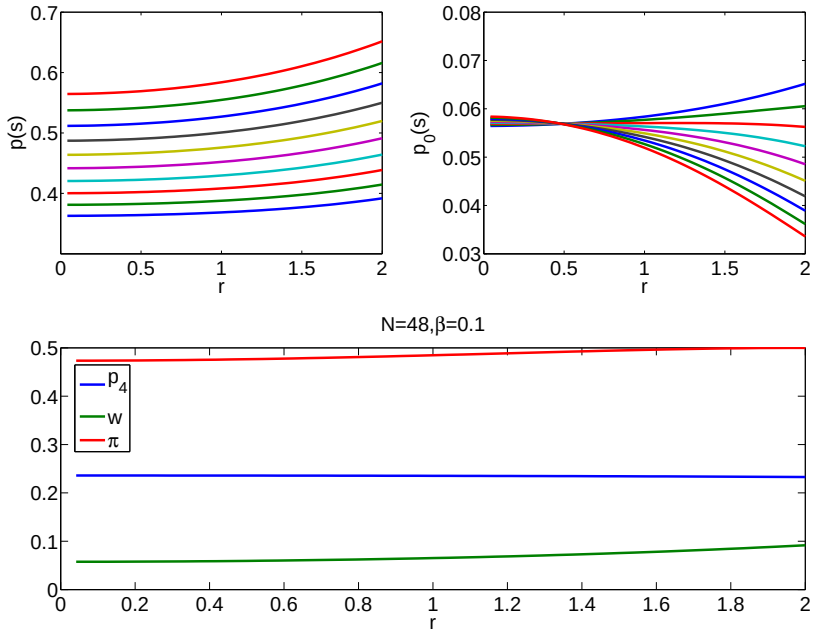

Figure 3: radial symmetric solutions for (11) with $\beta = 0.1$

We now turn our attention to determining stability of the quasi steady state solutions. Since we are considering the local stability of the quasi steady state solutions, we drop the higher order terms in the system. Assume

$$\partial\Omega : r = R^0 + \epsilon R^1 + O(\epsilon^2),$$

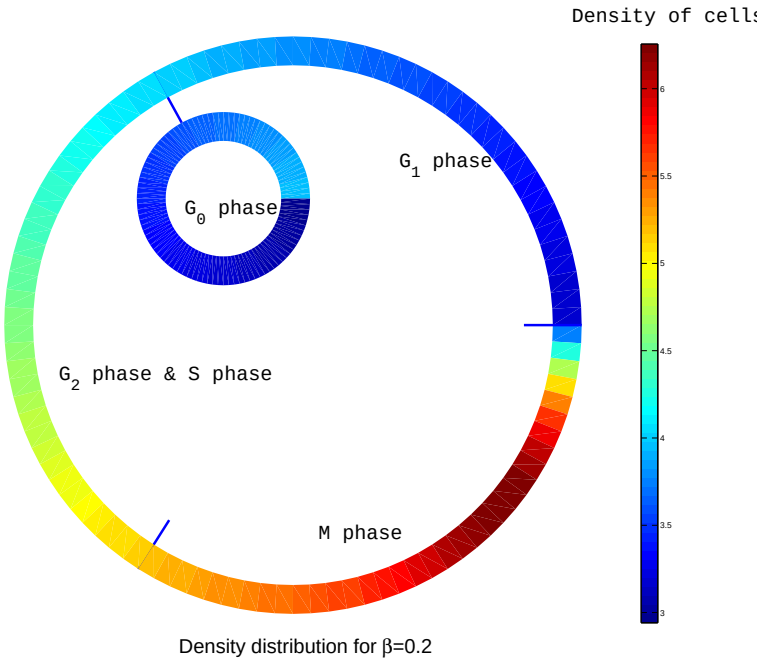

Figure 4: Density distribution

and

$$
\begin{aligned}
p &= p^0 + \epsilon p^1 + O(\epsilon^2),\\
p_0 &= p_0^0 + \epsilon p_0^1 + O(\epsilon^2),\\
p_4 &= p_4^1 + \epsilon p_4^1 + O(\epsilon^2),\\
\pi &= \pi^0 + \epsilon \pi^1 + O(\epsilon^2),\\
w &= w^0 + \epsilon w^1 + O(\epsilon^2).
\end{aligned}
$$

Then the linearized system is given by

$$
\begin{aligned}
\frac{\partial p^1}{\partial t} &+ \frac{\partial p^1}{\partial s} - \nabla p^1 \nabla \pi^0 - \nabla p^0 \nabla \pi^1 - p^1 \Delta \pi^0 - p^0 \Delta \pi^1 = \frac{\lambda w^0}{(1+w^0)p^1} - \frac{\lambda p^0 w^1}{(1+w^0)^2} \\
\frac{\partial p_0^1}{\partial t} &+ \frac{\partial p_0^1}{\partial s} - \nabla p_0^1 \nabla \pi^0 - \nabla p_0^0 \nabla \pi^1 - p_0^1 \Delta \pi^0 - p_0^0 \Delta \pi^1 = -\lambda_0 p_0^1 \\
\frac{\partial p_4^1}{\partial t} &- \nabla p_4^1 \nabla \pi^0 - \nabla p_4^0 \nabla \pi^1 - p_4^1 \Delta \pi^0 - p_4^0 \Delta \pi^1 = \mu_1 p^1(A) + \frac{\mu_2}{1-\mu_2} p^1(A_2) - \lambda_4 p_4^1 \\
& -\Delta \pi^1 = \frac{\lambda w^0}{1+w^0} Q^1 + \frac{\lambda w^1}{(1+w^0)^2} Q^0 - \lambda_0 Q_0^1 - \lambda_4 p_4^1 \\
& -\Delta w^1 + (Q^1 + Q_0^1) w^0 + (Q^0 + Q_0^0) w^1 = 0 \\
& w^1 = w_r^0 \text{ on } \partial\Omega(t) \\
& \pi_r^1 + \pi_{rr}^0 R_1 = 0 \text{ on } \partial\Omega(t) \\
& \pi^1 + \left(\frac{\gamma}{R^2} + \pi_r^0 \right) R_1 = 0 \text{ on } \partial\Omega(t).
\end{aligned}
$$

After discretizing on r direction, then the linearized system can be rewritten as

$$
\begin{pmatrix} \mathbf{p}^1 \\ \mathbf{p}_0^1 \\ \mathbf{p}_4^1 \\ \mathbf{0} \\ \mathbf{0} \end{pmatrix}_t = J(\mathbf{p}^0, \mathbf{p}_0^0, \mathbf{p}_4^0, \pi^0, \mathbf{w}^0) \begin{pmatrix} \mathbf{p}^1 \\ \mathbf{p}_0^1 \\ \mathbf{p}_4^1 \\ \pi \\ \mathbf{w} \end{pmatrix},
$$

where $J(\mathbf{p}^0, \mathbf{p}_0^0, \mathbf{p}_4^0, \pi^0, \mathbf{w}^0)$ is a matrix dependent on the quasi steady state solution $(\mathbf{p}^0, \mathbf{p}_0^0, \mathbf{p}_4^0, \pi^0, \mathbf{w}^0)$. Denote $J(\mathbf{p}^0, \mathbf{p}_0^0, \mathbf{p}_4^0, \pi^0, \mathbf{w}^0) = \begin{pmatrix} J_1 & J_2 \\ J_3 & J_4 \end{pmatrix}$, thus

$$
\begin{aligned}
\begin{pmatrix} \mathbf{p}^1 \\ \mathbf{p}_0^1 \\ \mathbf{p}_4^1 \end{pmatrix}_t &= (J_1 - J_2 J_4^{-1} J_3) \begin{pmatrix} \mathbf{p}^1 \\ \mathbf{p}_0^1 \\ \mathbf{p}_4^1 \end{pmatrix}, \\
\begin{pmatrix} \pi \\ \mathbf{w} \end{pmatrix} &= -J_4^{-1} J_3 \begin{pmatrix} \mathbf{p}^1 \\ \mathbf{p}_0^1 \\ \mathbf{p}_4^1 \end{pmatrix}.
\end{aligned}
$$

Therefore, the linear stability analysis is equivalent to the spectrum analysis of $(J_1 - J_2 J_4^{-1} J_3)$, i.e., the solution is stable if and only if each of the eigenvalues for $(J_1 - J_2 J_4^{-1} J_3)$ have negative real part. The maximum of real parts of eigenvalues of $(J_1 - J_2 J_4^{-1} J_3)$ is shown in Table 4. It shows that all the solutions are unstable since the constant β makes the model meaningless. The R_1 checkpoint is where eukaryotes typically arrest the cell cycle if environmental conditions make cell division impossible or if the cell passes into G_0 for an extended period. The constant β is regardless of such various environmental conditions so that this is not reasonable in real cell cycle.

Table 4: The maximum of real parts of eigenvalues of $(J_1 - J_2 J_4^{-1} J_3)$

β	$\max(\text{real}(\rho(J_1 - J_2 J_4^{-1} J_3)))$		
	$R = 1$	$R = 2$	$R = 3$
0.1	1.13	1.19	1.32
0.2	1.27	1.21	1.34
0.3	1.29	1.18	1.24
0.4	1.31	1.35	1.36
0.5	1.37	1.32	1.08
0.6	1.39	1.30	1.58
0.7	1.41	1.80	1.29
0.8	1.56	1.45	1.30

4.3 Control function β

For the constant β, the radially symmetric solutions we found are not stable by computing the spectrum of linearized system. The biological interpretation of this phenomenon is obvious since in this case β is left as a constant. Here we need to introduce a more biologically reasonable control function β. Using control on the signals from the microenvironment techniques, it is possible to find a β function that makes time dependent solutions close to the steady state solutions we found. Here $\beta(\mathbf{x})$ is a control

$$\{\beta : [0, R] \to [0, 1 - \mu_1]\}$$

subject to the system (11). This control function needs to satisfy the assumption in [17], i.e., $\beta(\mathbf{x})$ function is monotonically decreasing as $w(\mathbf{x})$ increases and monotonically increasing as $Q(\mathbf{x})$ increases. After many tries, we choose a control function β of Michaelis-Menten type:

$$\beta = \beta_0 + \gamma_1 \frac{Q(t) - Q_0}{\epsilon_1 + |Q(t) - Q_0|} - \gamma_2 \frac{w(t) - w_0}{\epsilon_2 + |w(t) - w_0|}, \tag{14}$$

where Q_0 is the steady state solution we found, and β_0 is the constant β corresponding to such steady state solution. The simulation is shown in Figure 5. This was accomplished by using a random perturbation of the steady state solution as the initial condition. The results demonstrate that the time dependent solution converges close to the steady state solution and oscillate near it. This control function β brings the cell to the end of the first checkpoint, signaling the $G_0 - G_1 - S$-phase transition.

5 Bifurcation problem

There results above imply, in particular, there exists a radially symmetric stationary solution with free boundary $r = R$ for any positive number R. While

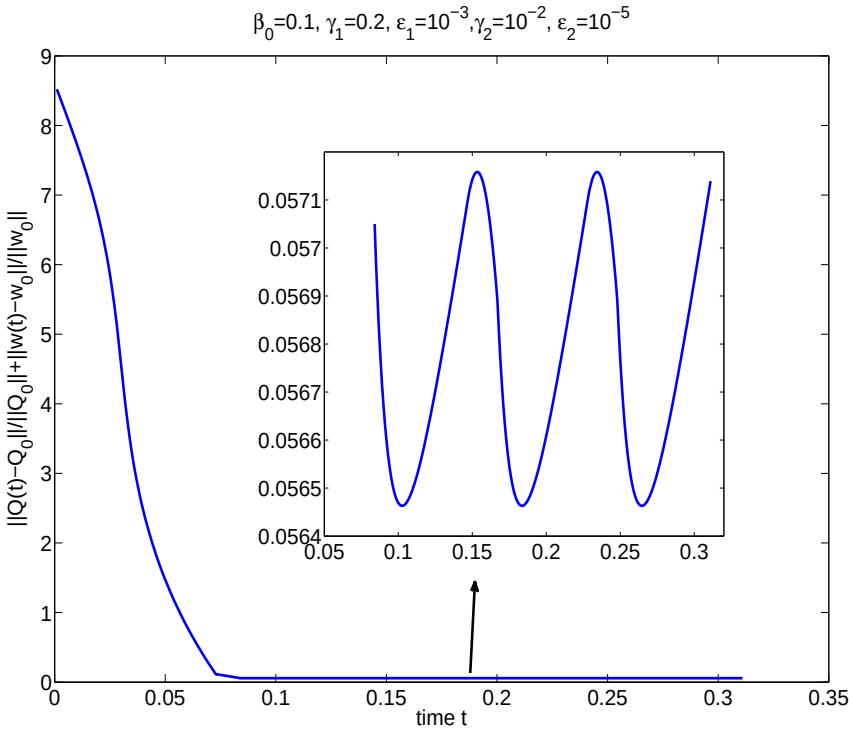

Figure 5: β function with control

tumors grown in vitro have a nearly spherical shape, tumors grown in vivo are usually not. It is therefore also very interesting to study the behavior of non-radially symmetric tumors. We utilized polar coordinates to discretize the system with the floating grid and third order finite difference scheme shown in [24, 26]. It is well known there exists branches of symmetry breaking stationary solutions for the systems in [24, 26]. However, we don't know whether there exists bifurcation or not for the system (11). One goal of this paper is to numerical algorithm to compute the bifurcation points if there are. Moreover, this algorithm can also numerically find the other branches arising from these bifurcation points.

5.1 Numerical verification for bifurcation

Bifurcation theory has been widely studied in nonlinear PDEs. The existence of bifurcation points on given solution curves can be established by giving small perturbations of source solutions. Based on the Crandall-Rabinowitz theorem, here we propose an algorithm for numerically verifying the bifurcation points.

This algorithm can be applied to complicated systems.

Algorithm 1: Bifurcation Verification Algorithm

Input : The parametric discetized system $F(x, \beta)$, where the parameter $\beta \in [\beta_0, \beta_1]$.

Output: Bifurcation points β^i, and the other branches across β^i.

Step 1: Homotopy track with respect to β, i.e., $\beta = t\beta_0 + (1-t)\beta_1$, and monitor the condition number of the Jacobian matrix $JF(x, \beta)$.

Step 2: Compute the below deflate system with the initial points whose condition number blow up in previous step and denote the solutions as (x^i, β^i, ξ^i), $i = 1, \cdots, l$.

$$\mathcal{D}(x, \beta, \xi) = \begin{bmatrix} F(x, \beta) \\ JF(x, \beta)\xi \\ \mathcal{L}(\xi) \end{bmatrix}$$

where $\mathcal{L}(\xi)$ is a general linear system.

Step 3: **for** $i = 1, \cdots, l$ **do**

- Compute the co-rank of $JF(x^i, \beta^i)$, if it is greater than 1, (x^i, β^i) is not a bifurcation point and continue with $i = i + 1$.
- Exact $n-1$ columns of $JF(x^i, \beta^i)$ such that they form a basis of $Im\ \big(JF(x^i, \beta^i)\big)$, denote as $y_1, y_2, \cdots, y_{n-1}$.
- Compute the kernel of the matrix $[JF_\beta(x^i, \beta^i)\xi^i, y_1, y_2, \cdots, y_{n-1}]$. If it is not an empty set, thus (x^i, β^i) is not a bifurcation point and continue with $i = i + 1$.
- Compute the other branch using the **TangentCone** algorithm in [24].

In this algorithm, Step 1 is the traditional path tracking of numerical algebraic geometry. Step 2 is to compute the bifurcation point with the deflate system. The Jacobian matrix $JF(x, \beta)$ is corresponding to the Frechét derivative $f_x(x, \beta)$. In step 3, we examined the conditions of the Crandall-Rabinowitz theorem in the first three sub-steps:

(i). $F(0, \mu) = 0$ for all μ in a neighborhood of μ_0,

(ii). Ker $F_x(0, \mu_0)$ is one dimensional space, spanned by x_0,

(iii). $F_{\mu x}(0, \mu_0)x_0 \notin Y_1$.

In the last sub-step of Step 3, the other branches arising from these bifurcation points are computed by TagentCone algorithm. We demonstrate this algorithm using the system (11) in next subsection.

5.2 Nonradial symmetric solution

According to bifurcation verification algorithm, we find two bifurcation points for the system (11) by tracking the radial symmetric branch with respect to the parameter β and verify the conditions in Step 3. The TagentCone Algorithm in Step 3 is to approximate the local tangent cone. This describes the tangent directions of the solution branches at the bifurcation. After computing the tangent direction for the nonradially-symmetric solution branch, the last step is to track along that solution branch using the tangent direction as a first order description of the solution branch locally. After successfully moving off of the bifurcation point and onto a smooth point on the solution branch, standard path tracking is used to track along the solution branch. Figure 6 shows pictorially demonstrates the local behavior of the solution branches which were computed using $N_R = 24, N_\theta = 10, N_S = 10$. Figure 7 shows the nonradial solutions in each direction along the nonradially-symmetric solution branches with ϵ function defined in [26]. More nonradial symmetric solutions and path tracking of radial symmetric branches are available at www.nd.edu/∼whao/cell_cycle.html.

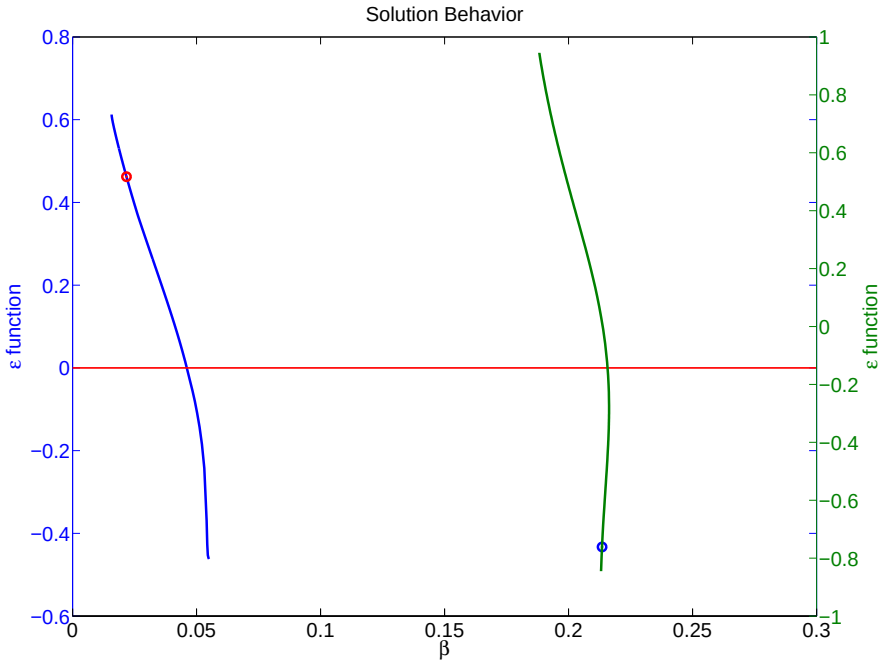

Figure 6: Solution Behavior

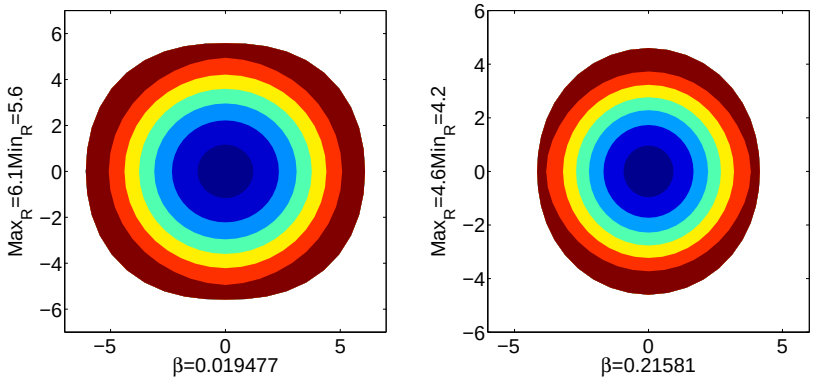

Figure 7: Nonradial solutions

5.3 Control on nonradial symmetric solutions

Similar to section 4.3, we apply the control function $\beta(\mathbf{x})$ of Michaelis-Menten type instead of constant function β in order to make the nonradial steady state solution converges close to the steady state solution and oscillate near it shown in Figure 8. The control function used is of the same form (14) with different values of parameters $\gamma_1, \gamma_2, \epsilon_1, \epsilon_2$.

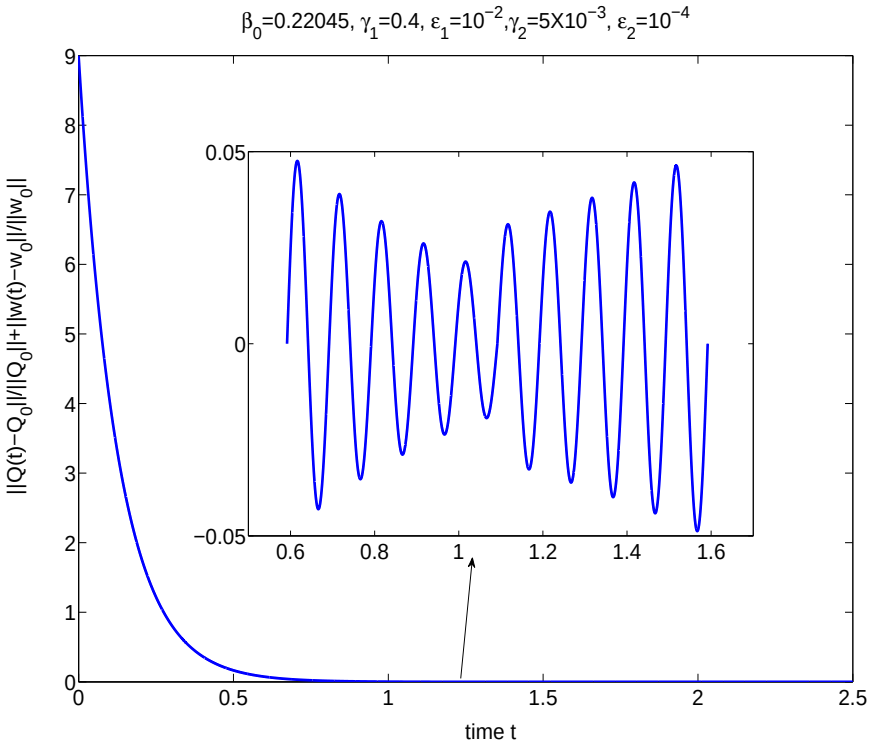

Figure 8: β function with control for non-radial solution

6 Conclusion

These results are based on a multiscale model with two time scales: the usual time t, and the running time of cells in each phase of the cell cycle. The model equations depend upon mass conservation for cell populations and on a diffusion equation for the oxygen. The growth or shrinkage of a tissue depends on a decision that individual cells make whether to proceed directly from the restriction point R_1 in G_1 phase to S phase, or whether to go first into quiescent state. First, we combine a finite difference discretization of the radial symmetric case

of the model and numerical algebraic geometric methods to solve polynomial system and obtain the radial symmetric solution. Then by tracking the parameter β, the non-trivial radial symmetric solutions are found when $\beta > 0$. A control function β is introduced and used to archive the quasi-stationary solutions. We also proposed a numerical algorithm to verify bifurcation point and found non-radial branches for the quasi-steady state system.

7 Acknowledgement

We would like to express our thanks to Professor Avner Friedman whose valuable comments and suggestions helped greatly to improve this article.

References

[1] B.P. Ayati, G.F. Webb, and A.R.A. Anderson, Computational methods and results for structured multiscale models of tumor invasion, *Multiscale Model. Simul.*, Vol. 5, 1–20, (2005).

[2] D.J. Bates, J.D. Hauenstein, A.J. Sommese, and C.W. Wampler, Bertini: Software for numerical algebraic geometry. Available at www.nd.edu/∼sommese/bertini.

[3] D.J. Bates, J.D. Hauenstein, A.J. Sommese, and C.W. Wampler, Software for numerical algebraic geometry: a paradigm and progress towards its implementation. In *Software for algebraic geometry, IMA Vol. Math. Appl.*, Vol. 148 1–14, (2008)

[4] D.J. Bates, J.D. Hauenstein, A.J. Sommese, and C.W. Wampler, Adaptive multiprecision path tracking, *SIAM J. Numer. Anal.*, Vol. 46, 722–746, (2008).

[5] D.J. Bates, J.D. Hauenstein, A.J. Sommese, and C.W. Wampler, Stepsize control for adaptive multiprecision path tracking, *Interactions of Classical and Numerical Algebraic Geometry, D. Bates, G. Besana, S. Di Rocco, and C. Wampler (eds.), Contemporary Mathematics*, (2009).

[6] B. Bazally and A. Friedman, Global existence and asymptotic stability for an elliptic-parabolic free boundary problem: an application to a model of tumor growth, *Indiana Univ. Math. J*, Vol 52, 1265–1304, (2003).

[7] A. Burton, Rate of growth of solid tumors as a problem of diffusion, *Growth*, Vol. 30, 157–176, (1966).

[8] H. Byrne and M. Chaplain, Growth of nonnecrotic tumors in the presence and absence of inhibitors, *Math. Biosci.*, Vol. 130, 151–181, (1995).

[9] H. Byrne and S. Gourley, The role of growth factors in avascular tumour growth, *Math. Comput. Modelling*, Vol. 26, 35–55, (1997).

[10] M. Chaplain, Avascular growth, angiogenesis and vascular growth in solid tumours: The mathematical modelling of the stages of tumour development, *Math. Comput. Modelling*, Vol. 23, 47–87, (1996).

[11] M. Chaplain and N. Britton, On the concentration profile of a growth inhibitory factor in multicell spheroids, *Math. Biosci.*, Vol. 115, 233–243, (1993).

[12] V. Cristini, J. Lowengrub, and Q. Nie, Nonlinear simulation of tumor growth, *J. Math. Biol.*, Vol. 46, 191–224, (2003).

[13] M. Fontelos and A. Friedman, Symmetry-breaking bifurcations of free boundary problems in three dimensions, *Asymptotic Analysis*, Vol. 35, 187–206, (2003).

[14] A. Friedman and B. Hu, Bifurcation from stability to instability for a free boundary problem arising in a tumor model, *Arch. Rat. Mech. Anal.*, Vol. 180, 643–664, (2006).

[15] A. Friedman and B. Hu, The role of oxygen in tissue maintenance: a mathematical model, *Math. Mod. & Meth. in Appl. Sci.*, Vol. 18, 1409–1441, (2008).

[16] A. Friedman and B. Hu, Stability and instability of Liapunov-Schmidt and Hopf bifurcation for a free boundary problem arising in a tumor model. *Trans. Amer. Math. Soc.*, Vol. 360, 5291–5342, (2008).

[17] A. Friedman, B. Hu, and C.Y. Kao, Cell cycle control at the first restriction point and its effect on tissue growth, *J. Math. Biol.*, Vol. 60, 881–907, (2010)

[18] A. Friedman, A multiscale tumor model, *Interfaces Free Bound*, Vol. 10, 245–262, (2008).

[19] A. Friedman, A free boundary problem for a coupled system of ellipitc, parabolic and Stokes equations modeling tumor growth, *Interfaces and Free boundaries*, Vol. 8, 247–261, (2006).

[20] A. Friedman, Free boundary problems associated with multisacle tumor models, *Math. Model. Nat. Phenom.*, Vol. 4, 134–155, (2009).

[21] A. Friedman and F. Reitich, Analysis of a mathematical model for growth of tumor, *J. Math. Biology*, Vol. 38, 262–284, (1999).

[22] H.P. Greenspan, Models for the growth of a solid tumor by diffusion, *Studies Appl. Math*, Vol. 52, 317–340, (1972).

[23] H.P. Greenspan, On the growth of cell culture and solid tumors, *Theoretical Biology*, Vol. 56, 229–242, (1976).

[24] W. Hao, J.D. Hauenstein, B. Hu, Y. Liu, A.J. Sommese, and Y.-T. Zhang, Bifurcation for a free boundary problem modeling the growth of a tumor with a necrotic core, *Nonl. Anal.: Real Worl. Appl.*, Vol. 13, pp. 694–709, (2012).

[25] W. Hao, J.D. Hauenstein, B. Hu, T. McCoy, and A.J. Sommese, Computing steady-state solutions for a free boundary problem modeling tumor growth by Stokes equation, *submitted. Available at www.nd.edu/∼sommese/preprints.*

[26] W. Hao, J.D. Hauenstein, B. Hu, and A.J. Sommese, A three-dimensional steady-state tumor system, *Appl. Math. Comp.*, Vol. 218, pp. 2661–2669, (2011).

[27] C.S. Hogea, B.T. Murray, and J.A. Sethian, Simulating complex tumor dynamics from avscular to vascular growth using a general level-set method, *J. Math. Biol.*, Vol. 53, 86–134, (2006).

[28] X. Li, V. Cristini, Q. Nie, and J. Lowengrub, Nonlinear three-dimensional simulation of solid tumor growth, *DCDS-B*, Vol. 7, 581–604, (2007).

[29] D.J.S. McElwain, and G.J. Pettet, Cell migration in multicell spheroids: Swimming against the tide, *Bull. Math. Biol.*, Vol. 55, 655–674, (1993).

[30] G.J. Pettet, C.P. Please, M.J. Tindall, and D.L.S. McElwain, The migration of cells in multicell tumor spheroids, *Bull. Math. Biol.*, Vol. 63, 231–257, (2001)

[31] A.J. Sommese and C.W. Wampler,The numerical solution of systems of polynomials arising in engineering and science. *World Scientific Publishing Co.*, Hackensack, NJ, 2005.

[32] K. Thompson and H. Byrne, Modelling the internalisation of labelled cells in tumour spheroids, *Bull. Math. Biol.*, Vol. 61, 601–623, (1999).

[33] X. Zheng, S.M. Wise, and V. Cristini, Nonlinear simulation of tumor necrosis, neoVascularization and tissue invasion via an adaptive finite-element/level-set method, *Bull. Math. Biol.*, Vol. 67, 211–259, (2005).